Monthly Notices
of the
ROYAL ASTRONOMICAL SOCIETY

Mon. Not. R. Astron. Soc. **416,** 2020–2026 (2011) doi:10.1111/j.1365-2966.2011.19174.x

Radio pulsar style timing of eclipsing binary stars from the All Sky Automated Survey catalogue

S. K. Kozłowski,[1,2⋆] M. Konacki[1,2⋆] and P. Sybilski[2⋆]

[1]*Astronomical Observatory, Adam Mickiewicz University, Poznań, Poland*
[2]*Nicolaus Copernicus Astronomical Center, Toruń, Poland*

Accepted 2011 June 2. Received 2011 June 2; in original form 2010 September 30

ABSTRACT

The light-time effect (LTE) is observed whenever the distance between the observer and any kind of periodic event changes in time. The usual cause of this change in the distance is the reflex motion about the system's barycentre due to the gravitational influence of one or more additional bodies. We analyse 5032 eclipsing contact (EC) and eclipsing detached (ED) binaries from the All Sky Automated Survey (ASAS) catalogue to detect variations in the times of eclipses which possibly can be due to the LTE effect. To this end we use an approach known from the radio pulsar timing where a template radio pulse of a pulsar is used as a reference to measure the times of arrivals of the collected pulses. In our analysis, as a template for a photometric time series from the ASAS, we use a best-fitting trigonometric series representing the light curve of a given EC or ED. Subsequently, an observed minus calculated (O−C) diagram is built by comparing the template light curve with light curves obtained from subsets of a given time series. Most of the variations we detect in O−C diagrams correspond to a linear period change. Three of the O−C diagrams show evidence of more than one complete LTE orbit. For these objects we obtain preliminary orbital solutions. Our results demonstrate that the timing analysis employed in radio pulsar timing can be effectively used to study large data sets from photometric surveys.

Key words: methods: numerical – binaries: eclipsing.

1 INTRODUCTION

The fact that the velocity of light is finite was not obvious till 1676 when Olaus Roemer carried out precise measurements of the times of eclipses of Jovian moons. He noted that Io eclipses were 'early' before opposition and 'late' after opposition when compared to the *Ephemerides Bononiensis Mediceorum Siderum*, a work by Cassini published in 1668. It includes tables of times of eclipses of Jovian moons, which were used to determine the differential longitude by simultaneous observations of the same eclipse from two places. Roemer's conclusion, though not a quantitative one, became a great discovery contradicting the Aristotelean thought. He provided scientists with the basics of the O−C (observed minus calculated) procedure (Sterken 2005b) and was the first one to analyse the effects caused by finite light speed, hereafter called the light-time effect (LTE).

Below we analyse the photometric data from the All Sky Automated Survey (ASAS; Pojmanski 2002). In Section 2, we present our method for analysing the timing variations. In Section 3, we show the outcome of applying our approach to the photometric series of 5032 eclipsing contact (EC) and eclipsing detached (ED) binaries from the ASAS. In Section 4, we discuss several interesting cases of most likely the LTE effect due to companions to the analysed systems and conclude in Section 5.

⋆E-mail: stan@ncac.torun.pl (SKK); maciej@ncac.torun.pl (MK); sybilski@ncac.torun.pl (PS)

2 AUTOMATED TIMING OF ECLIPSING BINARIES

Our basic concept of detecting timing variations in photometry of ED/EC in an automated way is based on the method used in radio pulsar timing. It consists of six steps which are shown as a block diagram in Fig. 1.

(i) *Get a raw data set.* It is assumed that a raw data set consists of n magnitudes (or fluxes), their errors and the times they were recorded.

(ii) *Prepare a template light-curve model.* A raw data set is phased with the known period and the parameters of a template light-curve model are calculated using the least-squares method. At this stage the period can be improved or corrected during the fitting process. This is often necessary for the ASAS data.

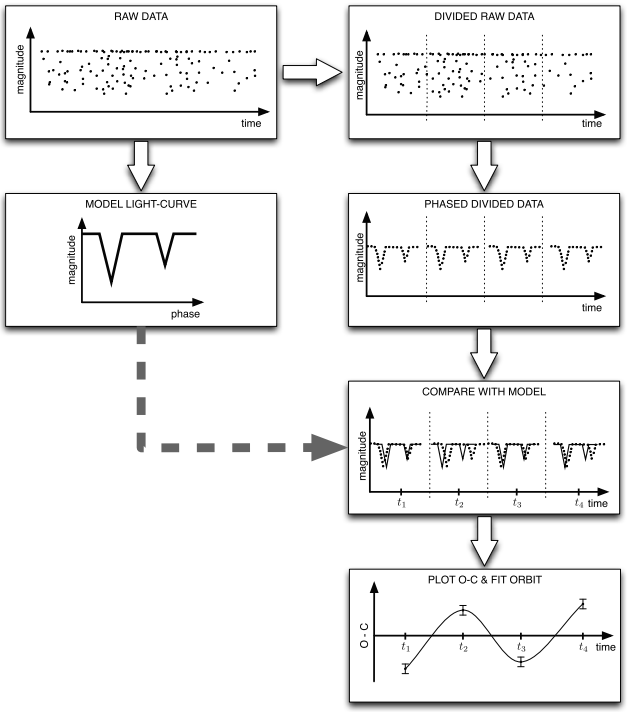

Figure 1. A block diagram describing our eclipse timing procedure.

(iii) *Divide a raw data set into subsets.* A raw data set is divided into M intervals. The intervals can be equal in terms of the number of data points they include or the time they span. The second variant was chosen in this paper. The intervals can be overlapping or have a non-repeating content. When implementing the first method, appropriate corrections must be applied when calculating the final formal errors due to a multiple usage of the same data points.

(iv) *Phase data in each interval.* Data points are phased separately in each interval using the new value of the period calculated during the creation of the model. The zero-point is retained for each interval. This way a *local light curve* is created and the mid-time of each interval is associated with it.

(v) *Compare with the template light-curve model.* The most important step in this procedure is the comparison of the *local light curves* with the template light-curve model. At this stage a one-parameter least-squares fit is performed in order to find the time shift between the two light curves.

(vi) *Plot an O−C diagram, fit an LTE orbit.* Finally, the collected O−C values can be plotted against time and, if possible, an orbit can be fitted.

2.1 A template light-curve model

We have tested two representations for a template light-curve model – a polynomial model and a harmonic model. We have decided to use a harmonic model. Such an approach, apart from providing a good model of the input data, enables us to conveniently adjust the initial period of a binary. The model is based on a Fourier series and involves fitting a trigonometric series to a raw photometric data set:

$$f(t) = \frac{a_0}{2} + \sum_{l=1}^{N} \left[a_l \cos\left(\frac{2\pi}{T} lt\right) + b_l \sin\left(\frac{2\pi}{T} lt\right) \right]. \quad (1)$$

Here, N has to be chosen so that the resulting light-curve model defined by the coefficients $a_0, \ldots, a_N, b_1, \ldots, b_N$ and the period T approximate the raw data as good as possible. Theoretically, the more harmonics are used (big N), the better the approximation will be. N has an upper limit though. Obviously, as a least-squares algorithm is used to fit $f(t)$, the number of parameters cannot exceed the number of data points used in a fit, i.e. $m = 2N + 2 < n$. Moreover, if m is close to n, the fit starts to approximate the data points. This is not a desired effect In our analysis, we used $N = 18$ which was found to be the best for the types of curves analysed. An example of a template light-curve model along with the original light curve is presented in Fig. 2. Though it might seem that a lower value of N would make the model less sensitive to erroneous data points, at the same time the real eclipses (especially deep and short ones) would not have been modelled well enough. Having the primary eclipse well modelled is crucial when searching for time shifts between the model and the local light curves. If one would have high-quality photometry, it would then be good to optimize the procedure and select N individually for each object. In order to carry out the least-squares fitting we used the Levenberg–Marquardt algorithm and its MINPACK[1] implementation.

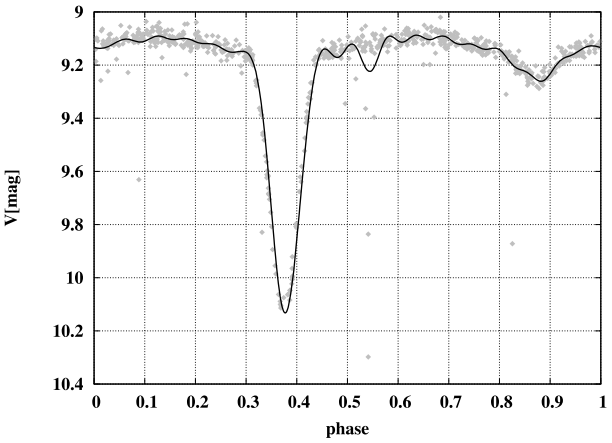

Figure 2. An example of a template light-curve model (solid line) calculated for ASAS 023539−4504.2 raw data. Note that the solid curve approximates the primary minimum very well despite oscillations visible between eclipses.

2.2 Calculating O−C

Having the light-curve model in the form of T and $a_0, \ldots, a_N, b_1, \ldots, b_N$ coefficients, it can be compared with local light curves in each interval. This is done by fixing the parameters describing the model in equation (1) and slightly modifying the formula by introducing a time-shift parameter t_O:

$$f_O(t) = \frac{a_0}{2} + \sum_{l=1}^{N} \left[a_l \cos\left(\frac{2\pi}{T} l(t - t_O)\right) + b_l \sin\left(\frac{2\pi}{T} l(t - t_O)\right) \right]. \quad (2)$$

Then, using the least-squares algorithm, $f_O(t)$ is fitted to local light curves with t_O being the only parameter. Effectively, t_O is the value of O−C at the given point of time. Collecting these for all intervals allows one to obtain an O−C diagram. Since equation (2) is fitted using the Levenberg–Marquardt algorithm as before, the formal errors of the obtained O−C values are derived from the covariance matrix, which, in this case, is a one-element matrix due to the fact that the fit has only one parameter.

[1] http://netlib.org/minpack/

Table 1. LTE search results: ASAS ED objects. The table lists the object's ID, the period value from the ACVS catalogue, a corrected period obtained during reference model computation. Four r values for five-, six-, seven- and eight-interval runs are given. The last column contains other IDs, if any.

ASAS ID	P[d] (ASAS)	P[d] (corrected)	r_5	r_6	r_7	r_8	Other ID
034746−0836.7	2.8764	2.876 8183	3.58	1.66	2.11	2.15	CD Eri
050205−2842.8	3.3023	3.302 4868	2.01	2.73	1.73	1.91	–
053727−7752.3	0.991 58	0.991 5804	3.14	2.74	2.25	1.92	–
070825−4433.2	1.8519	1.851 8267	2.17	1.97	1.15	2.24	–
071021−3324.6	1.657 725	1.657 7068	2.07	2.18	1.15	0.89	CI Pup
090039−4739.8	4.4045	4.404 7483	2.09	2.16	1.95	1.56	–
092456−3337.2	1.446 43	1.446 4050	2.42	2.23	2.45	1.15	SV Pyx
094542−4913.5	1.552 517	1.552 5371	3.00	3.38	3.27	1.86	DU Vel
111915−1949.7	2.3409	2.341 0108	3.80	3.71	3.10	2.33	RV Crt
121103−5040.3	1.9508	1.950 7456	2.28	2.05	1.87	1.58	NSV 05487
121158−5050.7	1.135 683	1.135 6929	2.16	2.03	1.63	2.15	NSV 05497
130155−5040.7	3.511 604	3.511 7345	2.96	2.03	1.88	1.94	NSV 06061
130856−7437.6	1.479 905	1.479 9275	2.44	2.49	2.75	2.21	–
132107−1936.4	3.042 031	3.042 0286	2.71	2.45	1.48	1.32	–
132402−6345.9	1.737 062	1.737 0648	5.64	5.36	4.32	4.09	–
132538−2025.0	0.478 49	0.478 4917	2.30	1.99	1.90	1.86	–
141035−4546.8	0.988 708	0.988 7115	2.04	1.86	1.85	1.42	–
143636−5124.8	1.453 13	1.453 0916	1.84	1.71	2.01	1.68	DT Lup
154645−2307.5	1.281 968	1.281 9585	2.87	2.43	2.00	2.36	–
161628−0658.7	2.446 109	2.446 1205	3.03	2.04	1.99	1.59	SW Oph
171519−3639.0	2.413 44	2.413 4785	2.05	1.50	1.47	1.99	V0467 Sco
174303−3222.3	2.192 577	2.192 5951	2.93	1.63	1.65	1.33	V0496 Sco
191350+1109.8	0.334 838	0.334 8409	1.76	1.58	2.04	2.02	–
193840−4500.6	1.351 87	1.351 8939	2.73	2.97	2.96	1.69	V0795 Sgr
200048−2833.4	1.665 189	1.665 1979	3.87	2.57	2.47	1.22	V1173 Sgr
205101−6341.5	2.5442	2.544 1900	2.68	1.23	1.01	1.16	BT Pav
213148−4502.7	1.880 496	1.880 5027	1.57	2.23	1.94	1.67	U Gru
215704−5606.0	0.454 887	0.454 8896	1.90	2.00	1.66	1.05	–
223621−1116.4	1.628 54	1.628 5257	2.70	1.36	1.71	2.02	–

2.3 Detection criterion

Inspecting visually every single O−C diagram is not practical; hence, in order to find binaries with significant timing variations we use the following timing activity parameter r:

$$r = \frac{S}{A} > r_{\min}, \tag{3}$$

where S is the standard deviation of the O−C values and A is the average error ($\Delta(O-C)$) of these values:

$$A = \frac{1}{M}\sum_{l=1}^{M} \Delta(O-C)_l. \tag{4}$$

Objects having r greater than a certain $r_{\min}$ are considered interesting. We applied the above criterion to data sets divided into five, six, seven and eight intervals. If an object passes the criterion at least once, it is considered interesting. Such objects are finally inspected visually.

3 TIMING VARIATIONS OF ED AND EC BINARIES FROM THE ASAS CATALOGUE

The ASAS Catalogue of Variable Stars (ACVS) is publicly available for download from the ASAS Project homepage.[2] We used its version 1.1 in this paper. The catalogue consists of 50 124 objects showing variability in brightness. Among them 2761 are uniquely classified as EC binaries and 2271 as ED binaries. Based on the original ACVS index file, we created two subindex files: one containing only EC binaries and the second one containing only ED binaries. This reduced the number of investigated light curves to 5032. In the analysis only an A-rated[3] photometry was taken into account. The results for ED are collected in Table 1. It lists 29 binaries. For this table we used $r_{\min} = 2.0$. The results for EC are tabulated in Table 2. It contains 44 objects. In this case we used $r_{\min} = 2.5$. The most frequent variation in O−C in both cases has a parabolic shape indicating a linear change in the period. The $r_{\min}$ threshold has been adjusted individually for each type of curves (ED and EC). In the case of contact binaries, the eclipses are generally shallower and less sharp than in the case of detached binaries – this results in different sensitivities of the algorithm in the two cases.

Recently, Pilecki, Fabrycky & Poleski (2007) have found EC binaries with high period change rates (HPCRs) in the ASAS data. They have published a list of 31 stars exhibiting large $\dot{P}$. 10 out of 44 objects listed in Table 2 have been detected by Pilecki et al. (2007). Of the remaining 21 HPCR objects, 12 were classified as other than EC; hence, they were not analysed by us. Finally, nine objects did not satisfy our criterion. In order to verify that the results obtained with our proposed algorithm are consistent with Pilecki et al. (2007), we compared objects with high $\dot{P}$ from the HPCR list with our timing measurements. This is demonstrated in Figs 3–4

[2] http://www.astrouw.edu.pl/asas/

[3] The ACVS rates the quality of each brightness measurement on a scale form A to D with A being the best and D the worst quality.

Table 2. LTE search results: ASAS EC objects. The table lists the object's ID, the period value from the ACVS catalogue, a corrected period obtained during reference model computation. Four r values for five-, six-, seven- and eight-interval runs are given. The last column contains other IDs, if any.

ASAS ID	P[d] (ASAS)	P[d] (corrected)	r_5	r_6	r_7	r_8	Other ID
002449−2744.3	0.313 67	0.313 6602	3.10	2.71	2.35	2.66	–
004240−2956.7	0.301 682	0.301 6864	3.49	3.15	2.29	3.25	–
030313−2036.9	0.334 978	0.334 9778	2.69	2.63	1.38	2.19	TU Eri
030315−2311.2	0.4566	0.456 6055	2.85	2.56	2.26	1.99	–
030617−6812.5	0.416 12	0.416 1200	4.35	4.23	3.77	3.97	NSV01054
032812−2503.5	0.315 501	0.315 5051	2.64	2.63	1.81	2.22	–
043046−4813.9	0.357 14	0.357 1467	3.59	3.56	2.19	3.06	–
050922−1932.5	0.270 842	0.270 8428	3.04	2.58	1.83	2.18	–
051114−0833.4	0.4234	0.423 4030	4.47	3.79	3.30	3.21	ER Ori
052313−0907.7	0.401 98	0.401 9834	4.40	3.69	2.21	2.38	–
054000−6828.7	0.362 22	0.362 2215	2.79	2.76	2.31	3.03	ASAS 054000−6828.6
055501−7241.6	0.343 841	0.343 8400	3.21	2.96	2.96	3.02	BV 435
060557−5342.9	0.463 63	0.463 6373	4.61	4.45	3.48	3.03	–
061654−4326.4	0.504 735	0.504 7355	3.98	3.51	2.14	2.88	–
062254−7502.0	0.257 704	0.257 7062	5.18	5.28	5.24	4.91	–
064047−8815.4	0.438 63	0.438 6210	4.31	3.62	3.06	3.56	–
065232−2533.5	0.418 634	0.418 6402	2.79	2.63	1.98	2.13	–
070225−2845.8	0.462 724	0.462 7283	5.89	4.82	4.49	4.36	–
070232−5214.6	0.407 338	0.462 7283	5.89	4.82	4.49	4.36	–
070943−0702.3	0.501 369	0.501 3665	3.58	3.05	2.28	2.28	–
071727−4007.7	0.320 267	0.320 2645	4.46	4.55	3.09	3.62	GZ Pup
074308−1915.5	0.403 302	0.403 3032	3.78	3.84	2.91	3.22	–
075809−4648.5	0.390 387	0.390 3834	5.01	5.38	3.81	4.47	NSV03836
082030−4326.7	0.370 78	0.370 7788	3.02	3.00	2.33	2.22	–
082456−4833.6	0.364 879	0.364 8710	6.88	5.69	4.86	3.67	–
083139−4227.5	0.302 677	0.302 6776	3.00	2.75	3.28	2.34	NSV04126
084304−0342.9	0.348 563	0.348 5601	3.70	3.63	4.09	3.34	–
093312−8028.5	0.406 071	0.406 0657	6.59	5.22	3.11	4.97	–
095048−6723.3	0.276 944	0.276 9428	2.64	2.74	2.04	2.30	NSV04657
102552−3224.3	0.337 06	0.337 0613	2.80	2.65	2.63	2.46	–
114757−6034.0	1.657 64	1.657 5598	4.25	3.59	3.11	3.16	SV Cen
123244−8726.4	0.338 519	0.338 5238	4.58	8.81	7.25	6.93	NSV 5654
131032−0409.5	0.311 251	0.311 2486	3.14	3.04	2.49	2.57	–
143103−2417.7	0.287 859	0.287 8586	3.19	2.75	2.34	2.51	–
144226−4558.1	0.251 557	0.251 5636	3.29	2.75	2.20	2.69	–
145124−3740.7	1.301 836	1.301 7970	2.93	2.78	2.37	2.62	V0678 Cen
150452−3757.7	0.374 131	0.374 1329	3.28	3.03	2.90	3.33	NSV06917
153152−1541.1	0.358 259	0.358 2558	2.36	2.55	3.46	3.73	VZ Lib
184644−2736.4	0.302 836	0.302 8365	3.47	2.70	2.24	2.64	–
195004−5146.7	0.875 46	0.875 4432	3.57	3.55	3.44	3.90	V0343 Tel
195350−5003.5	0.286 828	0.286 8259	6.96	5.85	4.40	5.92	NSV12502
202438−5244.0	0.315 93	0.315 9329	3.14	2.77	2.32	2.19	NP Tel
213519−2722.8	0.3689	0.368 9034	2.76	2.60	2.18	1.89	–
230749−2202.8	0.484 31	0.484 3096	6.19	6.33	4.78	4.52	–

by plotting the linear $\dot{P}$ (i.e. parabolic in O−C) trend from Pilecki et al. (2007) together with our timing measurements. We have also extended the O−C diagram from Pilecki et al. (2007) for VY Cet, a contact binary system with the well-known O−C variations. Qian (2003) studied this object and found the period of the third body to be 7.3 yr with a minimum mass of $0.62\,M_{\odot}$. Fig. 5 shows the original O−C diagram with our results overplotted.

4 ECLIPSING BINARIES WITH LTE ORBITS – ASAS 123244−8726.4, ASAS 075809−4648.5 AND ASAS 141035−4546.8

During a visual inspection of the detected timing variations we identified three interesting cases most likely corresponding to an LTE effect due to a third companion. We subsequently analysed them using a modified version of our approach. It differs from the original one described above in the way the intervals are chosen. Rather than setting the number of intervals, this time, the length of the intervals (in days) and the shift between them (in days) are used as parameters. This enables one to create overlapping intervals. For example, choosing a length of an interval of 300 d and setting the shift between intervals to 100 d produces 30 intervals assuming that the time-span is 3200 d. An important difference is that the data points are used multiple times for an O−C computation. This way it is possible to produce an infinite number of points in the O−C diagram having the same input data as in the standard algorithm. The statistical significance of these points is obviously appropriately lower than in the case of non-overlapping intervals and this must be taken into account when deriving formal errors. The main purpose

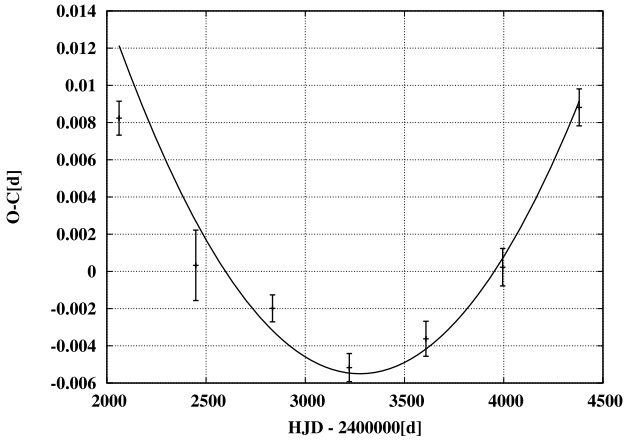

Figure 3. Timing variations of ASAS 060557−5342.9. The parabola corresponds to $\dot{P}$ from Pilecki et al. (2007).

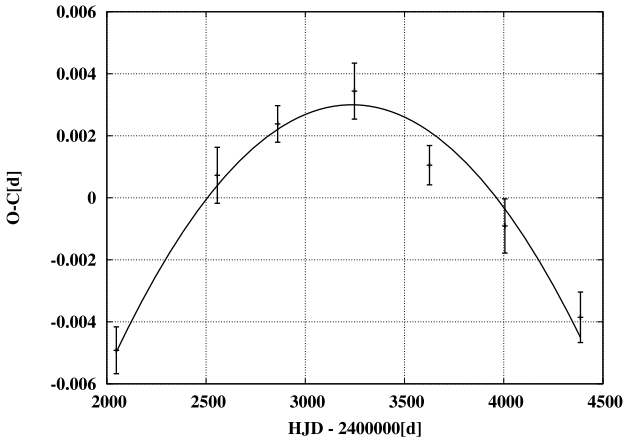

Figure 4. Timing variations of ASAS 160302−3749.4. The parabola corresponds to $\dot{P}$ from Pilecki et al. (2007).

of such an approach is to investigate how the O−C diagram looks between the points calculated using the standard algorithm and also how this influences the best-fitting LTE orbit.

ASAS 123244−8726.4, also known as NSV 5654 is an EC binary that has a period of $0^{\rm d}.338519$. It has been identified with high values of r reaching 8.81 in a six-interval run. The O−C plot is shown in Fig. 6. A linear trend introduced by an imprecise period

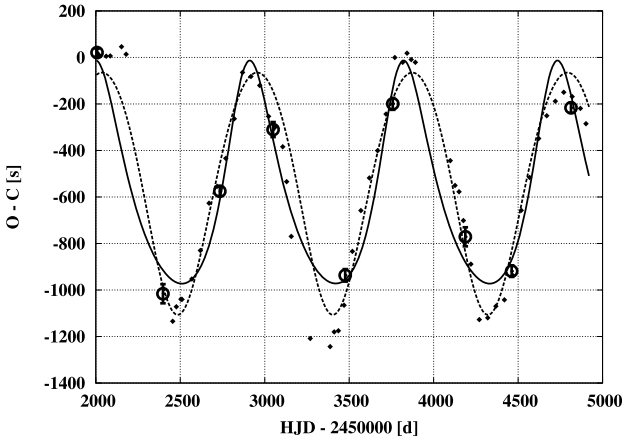

Figure 6. ASAS 123244−8726.4. The O−C diagram was obtained using the standard (circles with error bars and solid line) and the overlapping methods. Orbital solutions were fitted to both data sets.

was removed by applying a period correction obtained from an orbital fit which included a correction to the period *dP* as one of the parameters. The O−C diagram calculated using the new period shows evidence of an LTE orbit. Three complete cycles seem to be visible. The final orbital parameters are summarized in Table 3.

Another interesting EC object is ASAS 075809−4648.5 or NSV 03836. This binary, having a period of $0^{\rm d}.390383$, reveals periodic variability in the O−C diagram. As in the previous case, we used the standard (circles with error bars and solid line) and the overlapping method. Fig. 7 shows two sets of O−C data points as well as two corresponding orbital solutions. Parameters are shown in Table 3.

ASAS 141035−4546.8 is the only object among analysed ED systems that appears to exhibit periodic (O−C) variations with a period being clearly shorter than the data time-span. The eclipsing system has a period of $0^{\rm d}.988708$. Fig. 8 shows two sets of the O−C points as well as two corresponding orbital solutions. In the case of the orbit fitted to the points obtained with the standard method, a circular orbit was assumed. Table 3 provides the orbital parameters.

The above analysis of three interesting cases shows the usefulness of the proposed methods. The standard algorithm is well suited for detection and general O−C computation, while the second method based on overlapping intervals does the interpolation. It is not an interpolation in a strict mathematical sense though. There is no model (linear, cubic, spline, etc.) – O−C values are calculated according to the actual trend in the data set. As shown in the examples, such

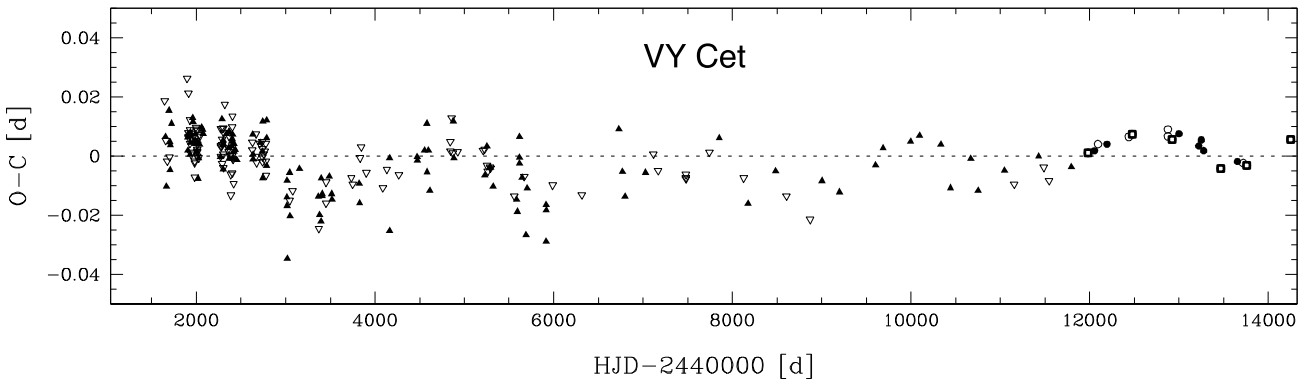

Figure 5. The timing variations of VY Cet. This O−C diagram is from Pilecki et al. (2007). Our timing variations are denoted with squares.

Table 3. LTE orbital parameters: period (P), projection of the semimajor axis a on the line of sight ($a \sin I$, I is the orbit's inclination), eccentricity (e), argument of periapsis (ω), mass function ($f(m_{1,2}, m_3)$) for ASAS 123244−8726.4, 075809−4648.5 and 141035−4546.8 computed using data from the standard and overlapping methods. RMS, χ^2 and the degrees of freedom (k) have been calculated for the standard method.

Parameter	Unit	Standard method	Overlapping method
		ASAS 123244−8726.4	
P	(d)	911 ± 5	918.4
$a \sin I$	(au)	0.961 ± 0.024	1.042
e	–	0.159 ± 0.019	0.055
ω	(°)	113 ± 8	0.98
T_0	(HJD)	$2450\,143 \pm 17$	2450 877
$f(m_{1,2}, m_3)$	($M_\odot$)	0.143 ± 0.011	0.179
RMS	(s)	67.8	–
χ^2	–	3.65	–
k	–	3	–
		ASAS 075809−4648.5	
P	(d)	1188 ± 27	1196
$a \sin I$	(au)	0.52 ± 0.04	0.57
e	–	0.131 ± 0.052	0.098
ω	(°)	84 ± 24	102
$f(m_{1,2}, m_3)$	($M_\odot$)	0.0133 ± 0.0031	0.0173
T_0	(HJD)	$2450\,328 \pm 80$	2450 234
RMS	(s)	40.77	–
χ^2	–	1.43	–
k	–	3	–
		ASAS 141035−4546.8	
P	(d)	1286 ± 120	1165
$a \sin I$	(au)	0.76 ± 0.13	0.84
e	–	0.0	0.32
ω	(°)	–	–
T_0	(HJD)	$2450\,292 \pm 122$	2450 154
$f(m_{1,2}, m_3)$	($M_\odot$)	0.035 ± 0.019	0.043
RMS	(s)	156.15	–
χ^2	–	2.23	–
k	–	2	–

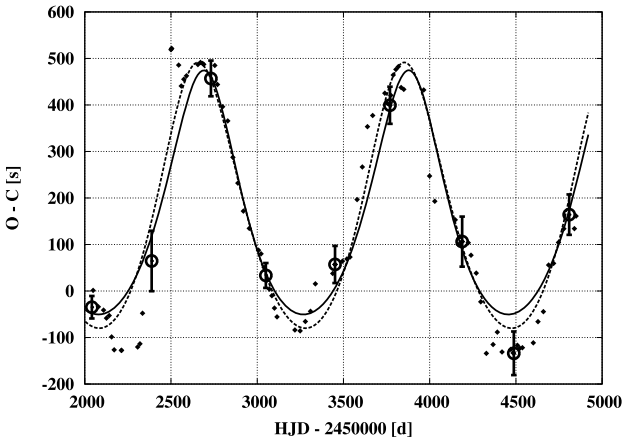

Figure 7. ASAS 075809−4648.5. The O−C diagram was obtained using the standard (circles with error bars and solid line) and the overlapping methods. Orbital solutions were fitted to both data sets.

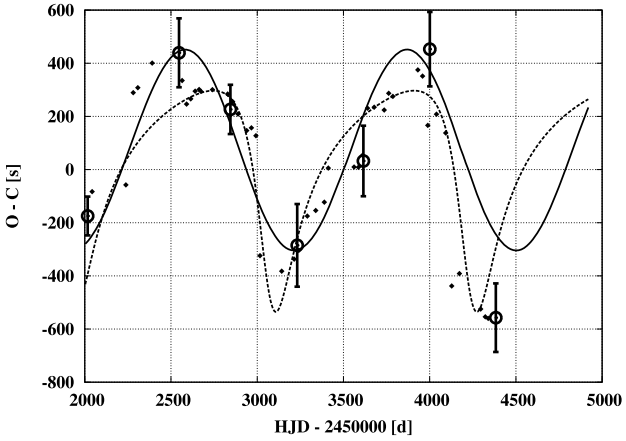

Figure 8. ASAS 141035−4546.8. The O−C diagram was obtained using the standard (circles with error bars and solid line) and the overlapping methods. Orbital solutions were fitted to both data sets.

interpolation can influence the shape of the fitted orbit. The eccentricity is the most sensitive parameter. $a \sin I$ and P do not differ much when comparing these two approaches.

5 CONCLUSIONS

ED and EC binaries were investigated. Altogether 5032 objects have been analysed in terms of the LTE. Results from five-, six-, seven- and eight-interval runs have undergone a test estimating the likelihood of interesting O−C variations. 29 detached and 44 contact binaries have passed the final visual tests. Most of the resulting O−C plots have a parabolic shape meaning a linear period increase or decrease. A few objects reveal third degree variations suggesting a long-period LTE orbit, of which only a short part is visible in the data set. Finally, three diagrams show evidence of LTE orbits that have periods shorter than the data's span. These objects have been precisely analysed using a modified version of the LTE-search algorithm. It uses overlapping intervals and generates more points on the O−C plot than the standard approach, thus revealing the possible shape of the orbit (without increasing the accuracy). Fitted orbits have semi-major axes smaller than 1 au and ≈3 yr periods.

Obtained O−C plots were compared with known literature data showing compatibility.

The proposed method is well suited for automated data pipelines due to its versatility. It can handle practically any long time-base photometry data and point out most irregularities in eclipse timing.

One thing worth mentioning is that, in general, dealing with O−C requires very precise periods. In our case, the periods came bundled with photometric data from the ASAS catalogue. If aliases, like ±10, 20, 30 per cent of the correct period, shall occur, the algorithm used to detect O−C variations will give a false signal. It must be therefore used with caution and understanding of the process.

Further simulation work regarding the influence of various light-curve parameters on the detection possibility is in progress.

ACKNOWLEDGMENTS

This work is supported by the Foundation for Polish Science through a FOCUS grant and fellowship, by the European Research Council through the Starting Independent Researcher Grant and by the Polish MNiSW grant no. N N203302035.

REFERENCES

Paczynski B., 1997, in Ferlet R., Maillard J.-P., Raban B., eds, Variables Stars and the Astrophysical Returns of the Microlensing Surveys: The Future of Massive Variability Searches. Editions Frontiéres, France, p. 357

Pilecki B., Fabrycky D., Poleski R., 2007, MNRAS, 378, 757

Pojmanski G., 2002, Acta Astron., 52, 397

Qian S., 2003, MNRAS, 342, 1260

Sterken C., 2005b, in Sterken C., ed., ASP Conf. Ser. Vol. 335, The Light-Time Effect in Astrophysics: Causes and Cures of the O−C Diagram. Astron. Soc. Pac., San Francisco, p. 181

This paper has been typeset from a TEX/LATEX file prepared by the author.